Predicting the evolution of fast chemical reactions in chaotic flows

Yue-Kin Tsang

Scripps Institution of Oceanography, University of California–San Diego, La Jolla, California 92093, USA

We study the fast irreversible bimolecular reaction in a two-dimensional chaotic flow. The reactants are initially segregated and together fill the whole domain. Simulations show that the reactant concentration decays exponentially with rate λ and then crosses over to the algebraic law of chemical kinetics in the final stage of the reaction. We estimate the crossover time from the reaction rate constant and the flow parameters. The exponential decay phase of the reaction can be described in terms of an equivalent passive scalar problem, allowing us to predict λ using the theory of passive scalar advection. Depending on the relative length scale between the velocity and the concentration fields, λ is either related to the distribution of the finite-time Lyapunov exponent of the flow or given in terms of an effective diffusivity which is independent of the small-scale stretching properties of the flow. For the former case, we suggest an optimal choice of flow parameters at which λ is maximum.

PACS number(s): 47.52.+j, 47.70.Fw, 05.45.−a, 82.40.Ck

I. INTRODUCTION

The effects of mixing on chemical reactions in fluids have long been recognized [1,2]. In many industrial and chemical processes, well-designed mixing efficiently brings reactants into contact [3], leading to increased product selectivity and higher reaction yields. Reactive mixing also plays a major role in other disciplines where various types of reactions are involved. Some examples are air pollution modeling [4], ozone hole modeling [5], and plankton population dynamics [6–8].

In this paper, we focus on the irreversible bimolecular reaction

$$A + B \rightarrow 2P, \qquad (1)$$

in which the two species A and B react and produce the inert product P. The initially segregated reactants together occupy the whole domain and are in contact along a material surface. The reaction is assumed to be fast and thus diffusion limited [9]. Fast bimolecular reaction appears in a wide range of processes including the removal of pharmaceutically active compounds during drinking water treatment [10] and the sulfur cycle in the marine boundary layer [11]. Although out of the scope of this paper, we mention another class of initial condition in which the two reactants are separated by a third inert medium [12]. Such configuration has important applications such as the parametrization of mix-down time in atmospheric chemical transport [13] and the estimation of fertilization rate in broadcast spawning [14].

We are interested in the time evolution of a bimolecular reaction in a two-dimensional incompressible flow that is Lagrangian chaotic, meaning that nearby fluid trajectories diverge from each other exponentially in time. In such systems, experiments [15,16] and numerical simulations [17,18] clearly demonstrate that the growth of product concentration, or equivalently the decay of reactant concentration, depends on the flow pattern. The exact shape of the decay varies among studies, especially at large time when the reaction is near completion. For the model we consider in this paper, numerical simulations show that the reactant concentration decays exponentially before it undergoes a transition to the algebraic law of classical kinetics in the late stage of the reaction.

Several theoretical works have made predictions of the decay rate of the reactant concentration. Using a steady strain flow $\boldsymbol{u} = (\alpha x, -\alpha y)$ in a lamellar model, Sokolov and Blumen [19] predicted that for random initial condition, the reactant concentration at first decays exponentially and then crosses over to power-law decay at long time. During the first phase, the exponential decay rate is $\alpha/2$. Károlyi and Tél [20] related the exponential decay of reactant concentration to a time-dependent effective fractal dimension [21,22] and expressed the decay rate in terms of the average Lyapunov exponent of the flow. Arratia and Gollub [16] showed in their experiment that the average Lyapunov exponent may be used to predict the time dependence of the mean product concentration for flows with different dynamical features. These results are in accord with the common belief that the stretching properties of the velocity field, usually characterized by an average Lyapunov exponent, have a strong influence on the progress of the reaction. However, as we shall see below, there are scenarios where the Lyapunov exponent is not the relevant quantity controlling the progress of the reaction. Specifically, when the flow scale is much smaller than the domain size, the reaction progresses much slower than estimates based on Lyapunov exponents.

Our analysis is based on the fact that for an infinitely fast reaction, the reactive mixing problem can be transformed [19,23] into the problem of a decaying passive scalar and the reactant concentration decay rate may be deduced from the variance decay rate in the equivalent passive scalar problem. Our numerical results explicitly establish the applicability of such passive scalar approximation to reactions of fast but finite rate. This lets us take advantage of recent advances in the theory for chaotic advection of passive scalars (see, for example, Refs. [24–29] and references therein). For the type of initial condition we consider here, where the longest length scale of the concentration field equals the domain size, we find that when the velocity varies on the same scale as the domain size, the progress of the reaction is controlled by the small-scale stretching characteristics of the flow. Fur-

thermore, it is necessary to take into account the fluctuation in the stretching statistics. On the other hand, if the velocity correlation length is much smaller than the domain size, the large-scale transport of the flow becomes the crucial and limiting factor. We make quantitative predictions of the reactant decay rate in both cases and verify them with numerical simulations.

In Sec. II, we formulate the advection-diffusion-reaction problem and present our flow model. Section III presents and discusses results from our numerical simulations for different flow parameters. In Sec. IV, we develop a theory for the reactant decay rate and compare its predictions to simulations. We discuss the special case where the stretching statistics are Gaussian and also suggest the existence of an optimal velocity correlation time at which the product growth rate is maximum. Section V concludes the paper.

II. MATHEMATICAL FORMULATION

A. Advection-diffusion-reaction equations

The interplay between advection, diffusion, and reaction may be described by microscopic, individual-based stochastic models [30–32]. The mean-field approximation to such many-body formulation usually gives rise to deterministic differential equations [33]. In the present work, we shall adopt such mean-field approach and use the following advection-diffusion-reaction equations as our model:

$$\frac{\partial a}{\partial t} + \boldsymbol{u} \cdot \nabla a = \kappa \nabla^2 a - \gamma ab, \tag{2a}$$

$$\frac{\partial b}{\partial t} + \boldsymbol{u} \cdot \nabla b = \kappa \nabla^2 b - \gamma ab, \tag{2b}$$

$$\frac{\partial p}{\partial t} + \boldsymbol{u} \cdot \nabla p = \kappa \nabla^2 p + 2\gamma ab. \tag{2c}$$

Here, $\boldsymbol{u}(\boldsymbol{x},t)$ is a two-dimensional incompressible velocity and $a(\boldsymbol{x},t)$, $b(\boldsymbol{x},t)$, and $p(\boldsymbol{x},t)$ are the concentration fields of A, B, and P, respectively. γ is the reaction rate constant and all reactants and product are assumed to have the same diffusivity κ. We consider a square periodic domain of side $2\pi L \times 2\pi L$. The initial condition is such that $a(\boldsymbol{x},0) = P_F$ in the right half of the domain and vanishes elsewhere while $b(\boldsymbol{x},0) = P_F \neq 0$ only in the left half. Here, $P_F \equiv \langle p(\boldsymbol{x},\infty)\rangle$ is the final average product concentration, where $\langle \cdot \rangle$ denotes spatial average over the whole domain. Conservation of matter implies

$$\langle p \rangle = P_F - 2\langle a \rangle, \tag{3}$$

$$\langle a \rangle = \langle b \rangle \tag{4}$$

for all time t.

B. Chaotic flow model

For the advection of reactants, we employ the following incompressible chaotic flow [24]:

$$\boldsymbol{u}(\boldsymbol{x},t)$$
$$= \begin{cases} \sqrt{2}U \cos[k_f y + \theta_1(n)]\hat{\imath}, & n\tau < t \leq \left(n+\frac{1}{2}\right)\tau \\ \sqrt{2}U \cos[k_f x + \theta_2(n)]\hat{\jmath}, & \left(n+\frac{1}{2}\right)\tau < t \leq (n+1)\tau, \end{cases} \tag{5}$$

where n is an integer. θ_1 and θ_2 are randomly chosen with uniform density on $(0,2\pi)$ and uncorrelated for different n. The characteristic scales of the flow are U, k_f, and τ.

We can characterize the stretching in a chaotic flow by the Lyapunov exponent. Consider two nearby fluid parcels initially at positions $\boldsymbol{x}_0$ and $\boldsymbol{x}_0 + \boldsymbol{\delta}_0$; the separation $\boldsymbol{\delta}(t)$ between them typically grows exponentially. We define the (maximum) finite-time Lyapunov exponent over a time interval t as

$$h(\boldsymbol{x}_0,t) = \max_{\boldsymbol{\delta}_0}\left\{\frac{1}{t}\ln\frac{|\boldsymbol{\delta}(t)|}{|\boldsymbol{\delta}_0|}\right\}, \tag{6}$$

where the maximum is taken over all orientations of $\boldsymbol{\delta}_0$. As $t \to \infty$, $h(\boldsymbol{x}_0,t)$ approaches the infinite-time Lyapunov exponent $\bar{h}$ for almost all $\boldsymbol{x}_0$. However, for finite time, h depends on $\boldsymbol{x}_0$ and have a distribution $\rho(h,t)$ that becomes more and more sharply peaked as t increases [34]. For sufficiently large t, the mean of the distribution will approximate the infinite-time Lyapunov exponent $\bar{h}$, i.e.,

$$\int_0^\infty \rho(h,t)h\,dh \to \bar{h}, \quad t \to \infty. \tag{7}$$

Figure 1(a) illustrates the time dependence of $\rho(h,t)$ for a typical set of parameters. These distributions are obtained by tracking the evolution of $16\,384^2$ individual $\boldsymbol{\delta}(t)$ initially scattered uniformly over the domain. From the large deviation theory [34,35], $\rho(h,t)$ obeys the large t asymptotic relation

$$\rho(h,t) = \sqrt{\frac{tG''(h)}{2\pi}}e^{-tG(h)}, \tag{8}$$

where $G(h)$ is independent of t. Moreover, $G(h)$ is concave upward, $G''(h) \geq 0$, with minimum value zero and $G(\bar{h}) = G'(\bar{h}) = 0$. Figure 1(b) shows the $G(h)$ corresponding to the $\rho(h,t)$ in Fig. 1(a). We see that $G(h)$ is indeed time independent at large t, thus we verify Eq. (8) for our flow model Eq. (5). Birch *et al.* [8] gave the following empirical formula for $\bar{h}$ as a function of (U,k_f,τ) for the model Eq. (5):

$$\bar{h} = Uk_f\Lambda(Uk_f\tau), \tag{9a}$$

$$\text{where} \quad \Lambda(z) = \frac{\ln(1+z^2/10+z^4/67)}{2z}. \tag{9b}$$

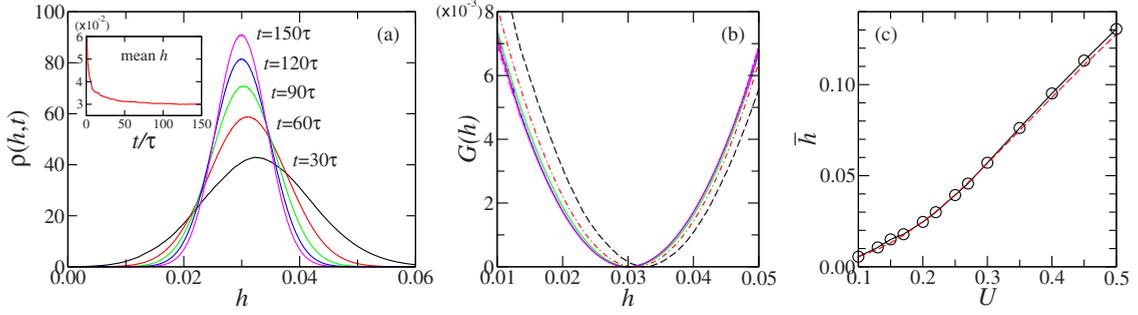Figure 1(c) plots $\bar{h}$, as obtained by Eq. (7), versus U and shows that the empirical formula works very well.

FIG. 1. (Color online) Stretching properties of the chaotic flow Eq. (5) with $U=0.22$ [in (a) and (b)], $k_f=1$, and $\tau=10$. (a) Probability density $\rho(h,t)$ of the finite-time Lyapunov exponent h. Inset shows the mean of the distribution approaching the infinite-time Lyapunov exponent $\bar{h}$. (b) The collapse of the function $G(h)$, defined in Eq. (8), as t increases. Broken curves represent earlier time and solid curves denote later times. (c) $\bar{h}$, approximated by Eq. (7), as a function of U. The dashed curve is the empirical formula Eq. (9).

Another quantity concerning our flow model that will be useful in our investigation is the single-particle effective diffusivity given by

$$\kappa_{\text{eff}} = \frac{\langle(\Delta x)^2\rangle}{2\tau} = \frac{\langle(\Delta y)^2\rangle}{2\tau} = \frac{U^2\tau}{8}, \quad (10)$$

where Δx and Δy are the x and y displacements of a particle during the time interval between $t=0$ and $t=\tau$, $\langle(\Delta x)^2\rangle$ and $\langle(\Delta y)^2\rangle$ are computed by averaging over the random angles θ_1 and θ_2.

C. Dimensionless parameters

We estimate the initial reaction time as $(\gamma P_F)^{-1}$ and the advection time as $(Uk_f)^{-1}$. The diffusion time across a length k_f^{-1} is taken as $(\kappa k_f^2)^{-1}$. We then define the Péclet number Pe and the Damköhler number Da for our problem as follows:

$$Pe = \frac{U}{\kappa k_f} \quad \text{and} \quad Da = \frac{\gamma P_F}{Uk_f}. \quad (11)$$

We are interested in fast reactions and small diffusivity so that

diffusion time $\gg$ advection time $\gg$ reaction time,

hence $Pe \gg 1$ and $Da \gg 1$. For example, taking parameter values similar to those used in the experiment of Ref. [16] $\kappa = 2 \times 10^{-5}$ cm^2 s^{-1}, $U=0.5$ cm s^{-1}, $k_f=0.5$ cm^{-1}, and setting $\gamma P_F=1$ s^{-1}, we have $Da=4$ and $Pe=5 \times 10^4$.

Rescaling length by k_f^{-1}, time by $(\gamma P_F)^{-1}$, velocity by U, and concentration by P_F, we write Eqs. (2a) and (2b) (and similarly for the equation of p) in its nondimensional form

$$\frac{\partial a}{\partial t} + Da^{-1}\boldsymbol{u} \cdot \nabla a = \kappa_*\nabla^2 a - ab, \quad (12a)$$

$$\frac{\partial b}{\partial t} + Da^{-1}\boldsymbol{u} \cdot \nabla b = \kappa_*\nabla^2 b - ab, \quad (12b)$$

where $\kappa_* \equiv (DaPe)^{-1}$ and now

$$\langle p\rangle = 1 - 2\langle a\rangle, \quad (13)$$

with $\langle p\rangle \to 1$ as $t \to \infty$. The nondimensional domain size, $2\pi k_f L$, controls the scale separation between the largest possible length scale of the concentration field, which is the same as the domain size L in our configuration, and the velocity length scale k_f^{-1}. We shall consider two distinct cases $k_f L \approx 1$ and $k_f L \gg 1$.

III. NUMERICAL RESULTS

Following Ref. [36], we solve the advection-diffusion-reaction equations for the concentration fields a and b, Eq. (12), using the pseudospectral method [37] with exponential time differencing [38]. Time stepping is the fourth-order Runge-Kutta scheme and the time step equals 0.005. We also incorporate the modification suggested in Ref. [39].

The parameters of the problem are κ_*, Da, and τ. We fix $\kappa_*=5 \times 10^{-6}$ throughout this paper. For results presented in this section, we take $\tau=10$ and vary Da. The effects of τ will be discussed in Sec. IV E.

A. Large-scale velocity: $k_f L = 1$

We first consider the case $k_f L = 1$. The grid size used is 1024^2. Figure 2 shows the time evolution of the average product concentration for different values of Da. The quantity $1-\langle p\rangle$ is obtained from $\langle a\rangle$ using Eq. (13) and can also be interpreted as the remaining fraction of reactant A (or B). Figure 3 displays snapshots of $a(\boldsymbol{x},t)$ and $b(\boldsymbol{x},t)$ for $1/Da =0.22$, illustrating the spatial structure of the concentration fields at different stages of the reaction.

Generally for all values of Da investigated here, the decay of $\langle a\rangle$, hence the progress of the reaction, is relatively slow at the beginning when the interface between concentration fields of the two reactants has short length and the reactants remain mostly segregated, as shown in the top row of Fig. 3.

After about 15% of either species of the reactant has been consumed; $\langle a\rangle$ (or $\langle b\rangle$) starts to decrease exponentially as shown in Fig. 2,

$$2\langle a\rangle = 1 - \langle p\rangle \sim \exp(-\lambda t). \quad (14)$$

Such decay continues until $\langle p\rangle$ reaches about 90% of its ultimate value. During this exponential decay phase, the
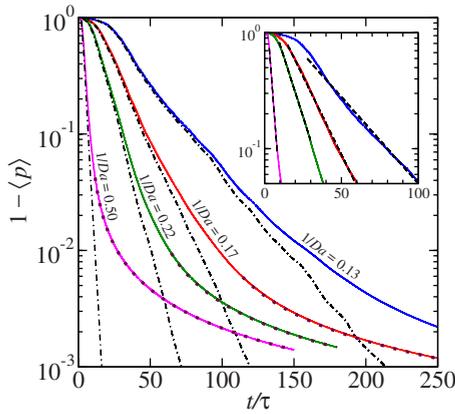
FIG. 2. (Color online) Time evolution of the average product concentration for $k_f L=1$ and different Da (solid curves). Dotted curves, which coincide with the solid curves at large t, are the classical kinetic law Eq. (15). Dot-dashed curves are $\langle |\phi| \rangle$ from the solution of the passive scalar problem Eq. (18a). The inset focuses on the exponential decay phase, where the dashed lines are least-squares fits used to estimate λ in Eq. (14).

stretching and folding action of the chaotic flow creates fine structures in the reactant concentration fields (see second row of Fig. 3). Increases in interface length and concentration gradients enhance diffusion and bring more reactants into contact. The reaction is fast and occurs mostly at the interface, so the overlap between a and b is still rather small. As
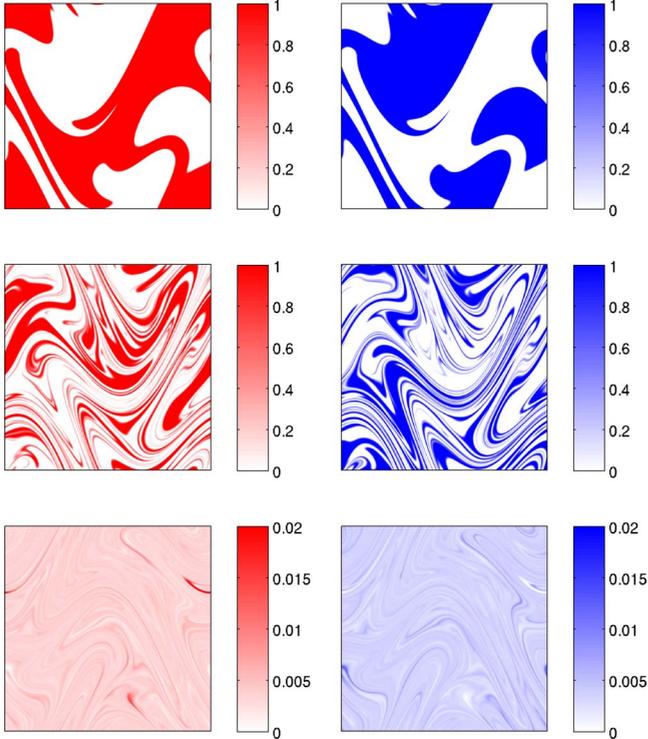

FIG. 3. (Color online) Snapshots of concentration fields of the reactants A (left) and B (right) at different stages of the reaction for $k_f L=1$ and $1/Da=0.22$. From top to bottom, time $t=3\tau$, 12τ, and 72τ. Note the different scale used in the bottom row. $\langle p \rangle \approx 0.018$, 0.347 and 0.993, respectively, for the three different times shown.
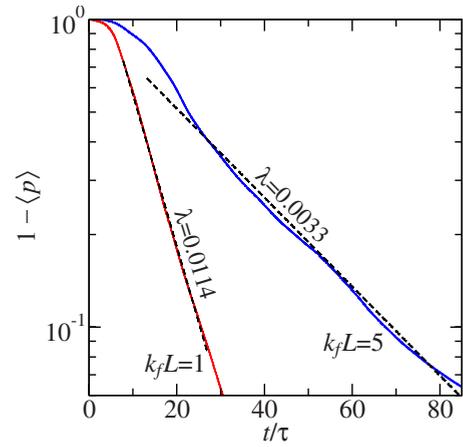

FIG. 4. (Color online) Comparison of the time dependence of the average product concentration for small-scale ($k_f L=5$) and large-scale ($k_f L=1$) advections, $Da=4$. Dashed lines are least-squares fits used to estimate λ in Eq. (14).

the majority of the product P is produced during the exponential decay phase, the decay rate λ is the most important indicator of how fast the reaction progresses. We shall present a theory to predict λ in Sec. IV.

All curves shown in Fig. 2 eventually level off as the reaction enters its final stage. At this time, the concentrations are low; a and b are fairly homogeneous and significantly overlap each other, as shown in the bottom row of Fig. 3. In this regime, we expect $\langle a \rangle$ to decay according to the classical chemical kinetic law (in our nondimensionalization)

$$\langle a(t) \rangle = \frac{\langle a(t_{cl}) \rangle}{1 + (t - t_{cl}) \langle a(t_{cl}) \rangle}, \tag{15}$$

which is obtained by neglecting the advection and diffusion terms in Eq. (12). We estimate t_{cl}, defined as the time after which classical kinetics applies, using the overlap integral

$$R(t) = \frac{\langle ab \rangle}{\sqrt{\langle a^2 \rangle \langle b^2 \rangle}}. \tag{16}$$

$R(t)$ increases noisily with time from 0 to 1 and measures the overlap between a and b. We determine t_{cl} by setting $R(t_{cl})=0.8$. Equation (15) is then plotted as dotted curves in Fig. 2 for $t \geq t_{cl}$ and is in excellent agreement with the simulation data.

B. Small-scale velocity: $k_f L=5$

We now turn to the situation where the velocity length scale is much smaller than the largest length scale of the concentration, specifically $k_f L=5$. We use the same velocity as in the previous section, but increase L by a factor of 5. Thus, Da and Pe in Eq. (11) and τ are unchanged. We use $Da=4$ as a representative case. The grid size is 5120^2. As shown in Fig. 4, with all other parameters the same, the reaction progresses much slower with small-scale advection. As before, an exponential decay phase exists during which Eq. (14) holds, albeit with a smaller λ. Notice that the probability density $\rho(h,t)$ is the same for both cases shown in
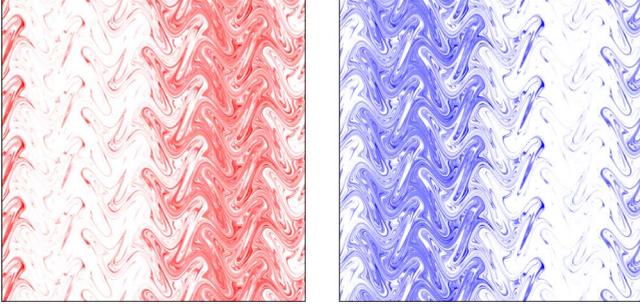
FIG. 5. (Color online) Snapshots of concentration fields of the reactants A (left) and B (right) for $k_f L=5$ and $Da=4$ at time $t=30\tau$. $\langle p \rangle \approx 0.641$ at this time instance. Values of a and b are between 0 and 1; darker shades represent higher concentration.

Fig. 4. This implies that the mechanism responsible for the exponential decay observed here with $k_f L=5$ is not related to the stretching properties of the flow, in contrast to the previous cases with $k_f L=1$.

The structure of the fields $a(\boldsymbol{x},t)$ and $b(\boldsymbol{x},t)$, shown in Fig. 5, also suggests a different mechanism is at work in a large domain. Throughout the course of the reaction, the amount of each species is much higher on one side of the domain than the other, resembling their respective initial condition. The two reactants move and come into contact through the filamentary structures penetrating into the high concentration region of each species. As a and b generally decrease in time, this pattern remains more or less unchanged. Note that the velocity becomes uncorrelated at length greater than $2\pi/k_f$, so the fluid parcels move like a random walk on the large scale. Hence, the transport of reactants from one side of the domain to the other is effectively diffusive and we anticipate that the effective diffusivity in Eq. (10) is the crucial property of the flow that controls the decay rate λ. We shall give a quantitative description of this picture in Sec. IV.

IV. THEORY

In this section, we apply the theory for the chaotic advection of passive scalars to predict the progress of a fast bimolecular irreversible reaction. In particular, we relate quantitatively the value of λ in Eq. (14) to the properties of the flow for both large-scale ($k_f L \approx 1$) and small-scale ($k_f L \gg 1$) velocities.

A. Relation to the passive scalar problem

Following earlier work, for example, Refs. [19,23], we introduce two functions,

$$\phi = a - b, \tag{17a}$$

$$\chi = a + b, \tag{17b}$$

which satisfy the equation of motions,

$$\frac{\partial \phi}{\partial t} + Da^{-1} \boldsymbol{u} \cdot \nabla \phi = \kappa_* \nabla^2 \phi, \tag{18a}$$

$$\frac{\partial \chi}{\partial t} + Da^{-1} \boldsymbol{u} \cdot \nabla \chi = \kappa_* \nabla^2 \chi + \frac{\phi^2 - \chi^2}{2}. \tag{18b}$$

For infinitely fast reactions, i.e., $Da \to \infty$, $a(\boldsymbol{x},t)$ and $b(\boldsymbol{x},t)$ never overlap, so $ab=0$ or equivalently $\phi^2=\chi^2$ for all $\boldsymbol{x}$ and t. Therefore, we have $a=(|\phi|+\phi)/2$ and $b=(|\phi|-\phi)/2$, which implies

$$\langle a \rangle = \langle b \rangle = \frac{1}{2}\langle |\phi| \rangle, \tag{19}$$

$$\langle p \rangle = 1 - \langle |\phi| \rangle. \tag{20}$$

The numerical results in Sec. III show that for a finitely fast reaction, the overlap between a and b is very small except during the late stage of the reaction. Thus, it is expected that until the reaction is near completion, Eq. (20) will be a good approximation for finite but large Da. We explicitly verify this by solving Eq. (18a) numerically and comparing $\langle |\phi| \rangle$ to $1-\langle p \rangle$. As shown in Fig. 2, the two quantities follow each other closely up until the end of the exponential decay phase. This observation allows us to understand the exponential behavior of $\langle p \rangle$ by studying the passive scalar problem for ϕ.

For a finitely fast reaction, the exponential decay phase ends when the passive scalar approximation fails. This failure is because the reaction rate is γ times the exponentially decreasing concentrations a and b. Thus, once the concentrations are sufficiently small, the reaction is no longer fast relative to diffusion, hence a and b start to overlap. This crossover happens at the time t_X when the diffusion term becomes comparable to the reaction term in Eq. (2). We can estimate t_X as follows. During the exponential decay phase, comparing strain against diffusion gives the width of a filament as $w \sim \sqrt{\kappa/\bar{h}}$. Balancing diffusion with reaction then yields

$$\kappa \frac{b}{w^2} \sim \gamma ab \tag{21}$$

or $\bar{h} \sim \gamma a$. But the concentration decays exponentially with $a(t_X) \sim P_F e^{-\lambda t_X}$ so that

$$t_X \sim \frac{1}{\lambda} \ln \frac{\gamma P_F}{\bar{h}}. \tag{22}$$

Substituting numerical values from our simulations into Eq. (22) shows that t_X indeed gives a good estimate to the time at which the decay starts to deviate from exponential.

B. Review of theory for passive scalar decay

There has been much development in the theory for chaotic advection of passive scalars recently. We now briefly review aspects of such theory that are relevant to our current study of reactive mixing. The main point is that the variance decay rate may be related to the probability distribution of the finite-time Lyapunov exponent of the flow [25] or to an effective diffusivity [26–28] depending on the size of $k_f L$, i.e., the velocity length scale relative to the largest possible scalar length scale.

Consider a passive scalar field ϕ in the same two-dimensional setup described in previous sections with governing equation Eq. (18a). The chaotic flow $\boldsymbol{u}$ is spatially smooth and single-scaled and $\langle\phi\rangle=0$. We also assume the absence of Kolmogorov-Arnold-Moser surfaces [40] and boundary effects [41,42]. In this situation, after initial transient, the system enters the "strange eigenmode" regime [24,43] in which ϕ exhibits statistically persistent spatial patterns while its amplitude decreases with time. Furthermore, the scalar variance decays exponentially [24]. These observations suggest the following form for the scalar field [8,25,43,44]:

$$\phi(\boldsymbol{x},t) = e^{-(s/2)t}\hat{\phi}(\boldsymbol{x},t), \quad (23)$$

where $\hat{\phi}(\boldsymbol{x},t)$ is statistically stationary and it follows that

$$\langle|\phi|^n\rangle \sim e^{-n(s/2)t}. \quad (24)$$

The existence of strange eigenmodes seems quite robust and Sukhatme and Pierrehumbert [44] give theoretical and numerical supports that Eqs. (23) and (24) are valid for both $k_fL\approx 1$ and $k_fL\gg 1$.

Much theoretical work focuses on the particular case of variance $(n=2)$ decay, $\langle\phi^2\rangle\sim e^{-st}$. It turns out that the mechanism of such decay depends on the value of k_fL [28,29]. When $k_fL\approx 1$, the decay is controlled by the small-scale stretching characteristics of the flow and the Lagrangian stretching theory [25,28] predicts that as $\kappa\rightarrow 0$,

$$s = \min_h[h + G(h)], \quad (25)$$

with $G(h)$ defined in Eq. (8). On the other hand, when $k_fL \gg 1$, it is the large-scale transport properties of the flow that determine the variance damping rate [26,27]. The gravest mode of ϕ then satisfies a diffusion equation with effective diffusivity κ_{eff} ($\gg\kappa$) given by Eq. (10). As a result,

$$s = \frac{\kappa_{\text{eff}}}{L^2}. \quad (26)$$

C. Predicting the decay rate λ

Because of Eq. (20), predicting the reactant decay rate λ in Eq. (14) is equivalent to determining the time dependence of $\langle|\phi|\rangle$ and Eq. (24) provides the answer

$$1 - \langle p\rangle \approx \langle|\phi|\rangle \sim e^{-(s/2)t}. \quad (27)$$

Therefore, using the results Eqs. (25) and (26),

$$\lambda \approx \frac{1}{2}\min_h[h + G(h)] \quad \text{when} \quad k_fL\approx 1 \quad (28)$$

and

$$\lambda \approx \frac{\kappa_{\text{eff}}}{2L^2} \quad \text{when} \quad k_fL \gg 1. \quad (29)$$

Figure 6 compares the theoretical prediction Eq. (28) with the decay rate measured in simulations for $k_fL=1$. The numerical decay rate is obtained by least-squares fits to the data
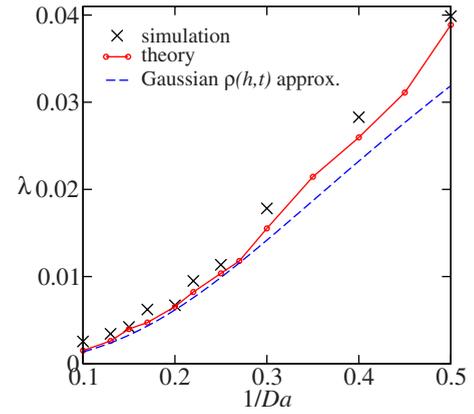

FIG. 6. (Color online) Comparison of the decay rate λ, defined in Eq. (14), for large-scale advection $k_fL=1$. Crosses are measured values from simulations described in Sec. III A. Circles are from the theory Eq. (28). The dashed curve uses the Gaussian approximation to $\rho(h,t)$ in the theory [Eq. (32)] and the formula Eq. (9) for $\bar{h}$.

(see inset of Fig. 2). To evaluate the right-hand side of Eq. (28), we use the procedure described in the Appendix, which circumvents the numerical estimation of $G(h)$. In general, we find good agreement between the theory and simulation results; the discrepancies are probably due to the finiteness of κ and γ in the simulations, since the theory is derived for the limiting case $\kappa\rightarrow 0$ and $\gamma\rightarrow\infty$. Furthermore, it is known that s converges rather slowly [28,29] to its zero diffusivity limit Eq. (25). This leads us to believe that the $\kappa\rightarrow 0$ limit is the more restrictive one. As for the case $k_fL=5$, with the parameter values used in Sec. III B, Eq. (29) predicts $\lambda=0.003\,125$, which agrees well with the numerical results shown in Fig. 4.

D. Flow with Gaussian $\rho(h,t)$

In this section, we give some results when the distribution of the finite-time Lyapunov exponent is Gaussian, specifically,

$$\rho(h,t) = \sqrt{\frac{t}{2\pi\sigma^2}} \exp\left[-t\frac{(h-\bar{h})^2}{2\sigma^2}\right], \quad (30)$$

where $\bar{h}$ is the mean and $\sigma/\sqrt{t}$ is the standard deviation of h. Strictly speaking, $h\geq 0$ as defined in Eq. (6). For the discussions in this section, we relax this restriction by dropping the maximization over the orientations of $\boldsymbol{\delta}_0$ in the definition. With this in mind, we can deduce that $\bar{h}=\sigma^2$ using the relation $\langle|\boldsymbol{\delta}(t)|^{-2}\rangle=\langle|\boldsymbol{\delta}_0|^{-2}\rangle$ proved by Zel'dovich *et al.* [45], here $\langle\cdot\rangle$ denotes ensemble average. Hence,

$$G(h) = \frac{(h-\bar{h})^2}{2\bar{h}}. \quad (31)$$
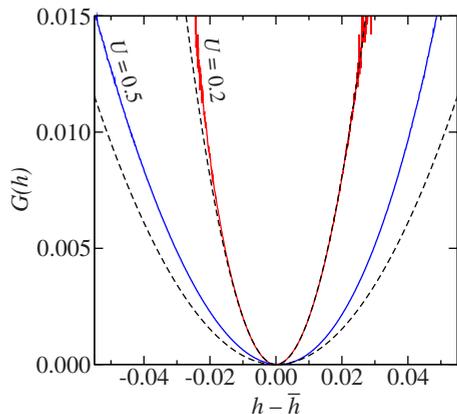
Then for $k_fL\approx 1$, Eq. (28) gives

FIG. 7. (Color online) Quadratic approximation Eq. (31) (dashed curves) for $G(h)$ of the flow Eq. (5) with different U. $k_f = 1$ and $\tau = 10$.

FIG. 8. (Color online) Decay rate λ, defined in Eq. (14), for different values of velocity correlation time τ, with $1/Da = 0.22$ and $k_f L = 1$. Crosses are measured values from simulations. Circles are from the theory Eq. (28). Dashed curve uses the Gaussian approximation to $\rho(h,t)$ in the theory [Eq. (32)] and the formula Eq. (9) for $\bar{h}$. λ reaches a maximum at $30 \lesssim \tau \lesssim 35$.

$$\lambda = \frac{\bar{h}}{4}. \tag{32}$$

The above result is generally true for any flow with Gaussian $\rho(h,t)$. For the flow Eq. (5), if we use the formula Eq. (9) for $\bar{h}$, we have a prediction for λ solely in terms of the flow parameters (U, k_f, τ), it is plotted as a dashed curve in Fig. 6. The Gaussian approximation is good when U is small but fails for large U. This is because while Eq. (31) is a very good approximation at small U, $\rho(h,t)$ becomes asymmetric when U is large and Eq. (31) does not fit the data well, as shown in Fig. 7.

The function $\Lambda(z)$ in Eq. (9b) has a global maximum [see Fig. 3(a) in Ref. [8]]. This means that in the case of $k_f L \approx 1$, for some given $U k_f$, there would be an "optimal" τ at which λ is maximum, assuming Eqs. (9) and (32) are applicable to the situation. We shall see in the next section that although Eq. (32) has limited validity, an optimal τ does exist.

E. Optimal velocity correlation time

We now explore how the progress of the reaction depends on the velocity correlation time τ given some fixed U and k_f. If $k_f L \gg 1$, the effective diffusion theory Eq. (29) implies that λ grows linearly with τ. When $k_f L \approx 1$, the dependence of λ on τ is less obvious. With $1/Da = 0.22$ and $k_f L = 1$, Fig. 8 shows that the value of λ measured in simulations increases linearly with τ before it levels off and reaches its maximum value at $30 \lesssim \tau \lesssim 35$. It then decreases rather slowly as we further increase τ. The small-scale stretching theory Eq. (28) agrees reasonably well with the numerical data and predicts the occurrence of a maximum at similar value of τ. The Gaussian approximation using Eqs. (9) and (32) shows a similar trend, but it does not agree with simulations quantitatively at large τ, when $\rho(h,t)$ is skewed. The interesting observation here is that the maximum of λ occurs at $U k_f \tau \approx 7$, which is suspiciously close to 2π. We thus speculate that the optimal choice for the velocity correlation time τ is roughly equal to the velocity correlation length $2\pi/k_f$ divided by the root-mean-square velocity U.
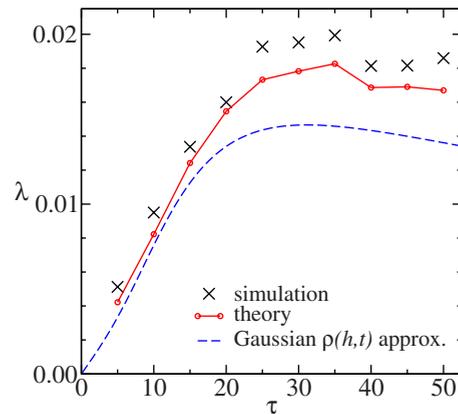
V. CONCLUSION

We study the evolution of a fast bimolecular reaction in a two-dimensional Lagrangian chaotic flow. For the range of parameters considered here, numerical simulations show that the reactant concentrations decay exponentially until the reaction reaches its final stage, at which point the decay becomes algebraic and proceeds according to the classical chemical kinetics.

Within the infinitely fast reaction approximation, which allows us to employ results from the theory for chaotic advection of passive scalars, we are able to make quantitative predictions on the reactant decay rate λ with good accuracy. The ratio of the velocity correlation length k_f^{-1} and the longest length scale L of the concentration field turns out to be an important parameter. When the two length scales are comparable, $k_f L \approx 1$, the stretching and folding of the fluid carry the reactants around the whole domain and bring them into close contact. The small-scale stretching of the flow controls the decay and λ is given by Eq. (28) in terms of the probability density of the finite-time Lyapunov exponent. For some fixed root-mean-square velocity U, λ attains its maximum value when the velocity correlation time τ roughly equals $2\pi/(U k_f)$. On the other hand, λ increases monotonically with U for any given τ. When $k_f L \gg 1$, the velocity varies on a much smaller scale than the gravest mode of the concentration field. As a result, the reactants are transported by eddy diffusion and the reaction progresses slower than the case of $k_f L \approx 1$. λ is given by Eq. (29) in terms of an effective diffusivity, independent of the small-scale stretching of the flow.

lated to this problem and suggestions that improved the paper. This work was supported by the National Science Foundation under Grant No. OCE07-26320.

APPENDIX: EVALUATION OF λ FROM EQ. (28)

While it is possible to evaluate the right-hand side of Eq. (28) from numerically computed $G(h)$ such as the ones shown in Fig. 1 [25], we employ the alternate method described in detail in Ref. [28], which is simpler to implement and more accurate. We recap the basic idea of this method here. The method is based on the following relation:

$$\langle e^{-ht} \rangle = \int \rho(h,t) e^{-ht} dh \sim \exp\{-\min_h [h + G(h)]t\}. \quad (A1)$$

Hence, using the ensemble of finite-time Lyapunov exponent $h_i(t)$ obtained by tracking large number of $\boldsymbol{\delta}(t)$ in Eq. (6), we estimate $\langle e^{-ht} \rangle$ as

$$\langle e^{-ht} \rangle_N \approx \frac{1}{N} \sum_{i=1}^{N} e^{-h_i(t)t}.$$

We then plot $\ln\langle e^{-ht} \rangle_N^{-1}$ versus t and obtained $\min_h[h + G(h)]$ as the slope of this curve. $N = 16\ 384^2$ in our calculation.

[1] J. C. Hill, Annu. Rev. Fluid Mech. **8**, 135 (1976).
[2] T. Tél, A. de Moura, C. Grebogi, and G. Károlyi, Phys. Rep. **413**, 91 (2005).
[3] J. Baldyga and J. R. Bourne, *Turbulent Mixing and Chemical Reactions* (Wiley, New York, 1999).
[4] B. Sportisse, Comput. Geosci. **11**, 159 (2007).
[5] S. Edouard, B. Legras, and V. Zeitlin, J. Geophys. Res., [Atmos.] **101**, 16771 (1996).
[6] C. López, Z. Neufeld, E. Hernández-García, and P. H. Haynes, Phys. Chem. Earth, Part B **26**, 313 (2001).
[7] A. P. Martin, Prog. Oceanogr. **57**, 125 (2003).
[8] D. A. Birch, Y.-K. Tsang, and W. R. Young, Phys. Rev. E **75**, 066304 (2007).
[9] A. A. Ovchinnikov, S. F. Timashev, and A. A. Belyy, *Kinetics of Diffusion Controlled Chemical Processes* (Nova Science Publishers, Commack, New York, 1989).
[10] M. M. Huber, S. Canonica, G.-Y. Park, and U. von Gunten, Environ. Sci. Technol. **37**, 1016 (2003).
[11] R. von Glasow, Atmos. Chem. Phys. **6**, 3571 (2006).
[12] J. P. Crimaldi, J. R. Cadwell, and J. B. Weiss, Phys. Fluids **20**, 073605 (2008).
[13] J. Thuburn and D. G. H. Tan, J. Geophys. Res., [Atmos.] **102**, 13037 (1997).
[14] J. P. Crimaldi and H. S. Browning, J. Mar. Syst. **49**, 3 (2004).
[15] O. Paireau and P. Tabeling, Phys. Rev. E **56**, 2287 (1997).
[16] P. E. Arratia and J. P. Gollub, Phys. Rev. Lett. **96**, 024501 (2006).
[17] F. J. Muzzio and M. Liu, Chem. Eng. J. **64**, 117 (1996).
[18] R. Reigada, F. Sagués, I. M. Sokolov, J. M. Sancho, and A. Blumen, J. Chem. Phys. **105**, 10925 (1996).
[19] I. M. Sokolov and A. Blumen, Phys. Rev. Lett. **66**, 1942 (1991).
[20] G. Károlyi and T. Tél, Phys. Rev. E **76**, 046315 (2007).
[21] A. Wonhas and J. C. Vassilicos, Phys. Rev. E **65**, 051111 (2002).
[22] A. E. Motter, Y.-C. Lai, and C. Grebogi, Phys. Rev. E **68**, 056307 (2003).
[23] M. Giona, S. Cerbelli, and A. Adrover, J. Phys. Chem. A **106**, 5722 (2002).
[24] R. T. Pierrehumbert, Chaos, Solitons & Fractals **4**, 1091 (1994).
[25] T. M. Antonsen, Jr., Z. Fan, E. Ott, and E. Garcia-Lopez, Phys. Fluids **8**, 3094 (1996).
[26] G. A. Voth, T. C. Saint, G. Dobler, and J. P. Gollub, Phys. Fluids **15**, 2560 (2003).
[27] D. R. Fereday and P. H. Haynes, Phys. Fluids **16**, 4359 (2004).
[28] Y.-K. Tsang, T. M. Antonsen, Jr., and E. Ott, Phys. Rev. E **71**, 066301 (2005).
[29] P. H. Haynes and J. Vanneste, Phys. Fluids **17**, 097103 (2005).
[30] G. Zumofen, J. Klafter, and A. Blumen, Phys. Rev. A **44**, 8390 (1991).
[31] D. A. Birch and W. R. Young, Theor. Popul. Biol. **70**, 26 (2006).
[32] A. R. Missel and K. A. Dahmen, Phys. Rev. E **79**, 021126 (2009).
[33] M. Doi, J. Phys. A **9**, 1479 (1976).
[34] E. Ott, *Chaos in Dynamical Systems*, 2nd ed. (Cambridge University Press, Cambridge, England, 2002).
[35] R. S. Ellis, *Entropy, Large Deviations and Statistical Mechanics* (Springer-Verlag, New York, 1985).
[36] S. M. Cox, Physica D **199**, 369 (2004).
[37] A. Adrover, S. Cerbelli, and M. Giona, Comput. Chem. Eng. **26**, 125 (2002).
[38] S. M. Cox and P. C. Matthews, J. Comput. Phys. **176**, 430 (2002).
[39] A.-K. Kassam and L. N. Trefethen, SIAM J. Sci. Comput. (USA) **26**, 1214 (2005).
[40] A. Pikovsky and O. Popovych, Europhys. Lett. **61**, 625 (2003).
[41] S. W. Jones and W. R. Young, J. Fluid Mech. **280**, 149 (1994).
[42] M. Chertkov and V. Lebedev, Phys. Rev. Lett. **90**, 134501 (2003).
[43] B. J. Bayly, in *Nonlinear Phenomena in Atmospheric and Oceanic Sciences*, edited by G. F. Carnevale and R. T. Pierrehumbert (Springer-Verlag, New York, 1992), pp. 139–176.
[44] J. Sukhatme and R. T. Pierrehumbert, Phys. Rev. E **66**, 056302 (2002).
[45] Y. B. Zel'dovich, A. A. Ruzmaikin, S. A. Molchanov, and D. D. Sokoloff, J. Fluid Mech. **144**, 1 (1984).